Electronic Supplementary Material (ESI) for Journal of Materials Chemistry A.

Supplementary Information

Highly active Ta_2O_5 Microcubic Single Crystals: facet energy calculation, facile fabrication and enhanced Photocatalytic Activity of Hydrogen Production

Hao Tu [‡, a], Leilei Xu [‡, a], Fangzhi Mou[a] and Jianguo Guan*[, a, b]

‡ These authors contributed equally.

[a] State Key Laboratory of Advanced Technology for Materials Synthesis and Processing, Wuhan University of Technology, 122 Luoshi Road, Wuhan, 430070, P. R. China.

[b] International School of Materials Science and Engineering, Wuhan University of Technology, 122 Luoshi Road, Wuhan, 430070, P. R. China.

Facet energy computation of Ta_2O_5

The β-Ta_2O_5 crystal structure model was taken for the facet energy calculation of Ta_2O_5. All operations were done in the first-principle theory module of CASTEP in Materials Studio. Generalized gradient approximation (GGA) of Perdew-Burke-Ernzerhof (PBE) was applied as the exchange-correlation potential.[1-5] Norm-conserving pseudo-potentials were employed. The cut-off energy for all slabs geometry optimization was 750 eV. All structures were fully relaxed. Different terminal slabs at possible cleaved positions are taken into consideration, resulting in two cases for {001} or {010}, and four cases for {100}. 14 Å thick vacuum layers and at least 7 layers of atoms for each slab were applied. Configurations of cutoff energy, *k*-point set and vacuum layer were identified by strict converge geometry optimization test in a criterion of difference below 0.01 eV/atom. As the bulk crystal is charge neutral and the slab models are all polar surfaces, according to the reconstruction mechanism such as ZnO polar surfaces,[6] terminal slabs are taken into combination to keep charge balanced, which results in one combination for {001} or {010}, and two combinations for {100}. The facet energy (γ) calculation is based on the following equations,[7]

$$\gamma = \frac{1}{2A}\left[G^{slab}(T,p,N_{Ta},N_O) - N_{Ta}\mu_{Ta}(T,p) - N_O\mu_O(T,p)\right] \tag{1}$$

$$2\mu_{Ta}(T,p) + 5\mu_O(T,p) = \mu_{Ta_2O_2}(T,p) = g^{bulk}_{Ta_2O_5}(T,p) \tag{2}$$

$$\gamma = \frac{1}{2A}\left[G^{slab}(T,p,N_{Ta},N_O) - \frac{1}{2}N_{Ta}g^{bulk}_{Ta_2O_5}(T,p) + \left(\frac{5}{2}N_{Ta} - N_O\right)\mu_O(T,p)\right] \tag{3}$$

For the evaluation of surface free energy (γ), equation (1) is used to calculate the structure in which O/Ta ratio is not consistent with 5/2. As for Ta_2O_5 structure, there is equation (2).

Therefore, we can use only one variable $\mu_O(T,p)$ to describe the surface free energy in equation (3). Each slab model has a unique linear correlation with $\mu_O(T,p)$. Next is to find the boundary conditions to determine the parameters in equation (3).

$$max\left[\mu_{Ta}(T,p)\right] = g^{bulk}_{Ta}(T,p) \tag{4}$$

$$min\left[\mu_O(T,p)\right] = \frac{1}{5}\left[g^{bulk}_{Ta_2O_5}(T,p) - 2g^{bulk}_{Ta}(T,p)\right] \tag{5}$$

$$max\left[\mu_O(T,p)\right] = \frac{1}{2}g^{gas}_{O_2}(T,p) \tag{6}$$

$$\gamma_{O-poor} = \frac{1}{2A}\left[G^{slab}(T,p,N_{Ta},N_O) - \frac{1}{5}N_O g^{bulk}_{Ta_2O_5}(T,p) + \left(\frac{2}{5}N_O - N_{Ta}\right)g^{bulk}_{Ta}(T,p)\right] \tag{7}$$

$$\gamma_{O-rich} = \frac{1}{2A}\left[G^{slab}(T,p,N_{Ta},N_O) - \frac{1}{2}N_{Ta} g^{bulk}_{Ta_2O_5}(T,p) + \frac{1}{2}\left(\frac{5}{2}N_{Ta} - N_O\right)g^{gas}_{O_2}(T,p)\right] \tag{8}$$

The maximum of Ta potentials is attained in metal Ta, equation (4). Since the Gibbs free energy of bulk Ta_2O_5 is considered as a const, the bottom of O potential is equation (5), which is transformed from equation (2) by citing the equation (4). Inducing the two boundary values into equation (3), we get equation (7) and (8), which are the range of surface free energy at predetermined temperature and pressure for poor and rich O environments. The facet energy function listed above is based on the Gibbs free energy of the system. However, there is only static state total energy excluding the vibrational contribution to Gibbs free energy in first-principle theory computing. Such vibrational contribution is about 10 meV·Å^{-2}, which doesn't influence the conclusion.[7] So the boundary conditions can be rewritten as follows. (E stands for total energy from first-principle theory computation)

$$\gamma_{O-poor} = \frac{1}{2A}\left[E^{slab}(V,N_{Ta},N_O) - \frac{1}{5}N_O E^{bulk}_{Ta_2O_5}(V) + \left(\frac{2}{5}N_O - N_{Ta}\right)E^{bulk}_{Ta}(V)\right] \tag{9}$$

$$\gamma_{O-rich} = \frac{1}{2A}\left[E^{slab}(V,N_{Ta},N_O) - \frac{1}{2}N_{Ta} E^{bulk}_{Ta_2O_5}(V) + \frac{1}{2}\left(\frac{5}{2}N_{Ta} - N_O\right)\mu^{gas}_{O_2}(T,p)\right] \tag{10}$$

Lastly, after citing values calculated by equation (9) and (10), the determined equation (3) of each terminal is drawn as lines with appointing $max\left[\mu_O(T,p)\right] = 0\ eV$ in Figure S5. The values attached in Figure 1 and Figure S6 are obtained at $\mu_O(T,p) =- 0.27\ eV$(p= 1 atm, T= 300 K).[7] The terminal combinations of the original facet structuresfacets structure with the lowest facet energies in {001}, {010} and {100} are chosen as the stable facets (Figure 1). The others are in Figure S6.

Electron density difference calculation

The β-Ta_2O_5 phase was taken as the model for the electron density difference calculation of Ta_2O_5. All the operations were performed in the first-principle theory module of CASTEP in Materials Studio. Nonlocal exchange Hartree-Fock (HF) was applied as the exchange-correlation potential.[1-5] Norm-conserving pseudopotentials were employed. The cut-off energy for all slabs geometry optimization was 600 eV.

Simulation and calculation of the transition from $TaO_{2.18}Cl_{0.64}$ to Ta_2O_5

For the simulation of the dynamic transition from $TaO_{2.18}Cl_{0.64}$ to Ta_2O_5, an approximate and simplified slab model (Figure S7) of $TaO_{2.18}Cl_{0.64}$ was applied in 950 K NVT (constant temperature and volume) dynamic simulation in the first-principle theory code of CASTEP Module. Generalized gradient approximation (GGA) of Perdew-Burke-Ernzerhof (PBE) was applied as the exchange-correlation potential.[1-5] Norm-conserving pseudopotentials were employed. The cut-off energy for the simulation was 300 eV. The k-point was set to gamma. The whole changing process of the model is shown in Video S1.

For the calculation of static energy, bulk amorphous models and intra-layer amorphous models were both investigated (Chart S2) and structured by means of Monte Carlo method in universal forcefield,[8] particularly, the amorphous atoms in the layer 2-dimensional space of the latter. Then, the bridge-O atoms were added between the layers to complete the model. The computation parameters were the same as that of the facet energy computation. The results are shown in Table S1.

Adsorption locator calculation

The H_2O adsorption locator speculation was carried out by Adsorption Locator Module based on Monte Carlo searches in Materials Studio.[9-12] All the facet slab models come from the Facet energy computation of Ta_2O_5 after full relaxation. This calculation can reveal the potential adsorption sites for H_2O molecule on the surface.

Preparation of Ta_2O_5 NHs

The Ta_2O_5 NHs were prepared according to the method reported by J. Y. Duan et al. According to J. Y. Duan's work,[13] 25 mg tantalum powders (black-color), 12.5 mL of 0.133 M hydrofluoric acid (HF) aqueous solution, and 4.0 mL of 30 wt % hydrogen peroxide (H_2O_2) solution were mixed and then transferred into a Teflon-lined autoclave with a volume of 25 mL, which was subsequently heated at 240 ^{o}C for 12 h in a box furnace. After the autoclave was cooled to room temperature naturally, the final white-color precipitates were separated, washed with ethanol for three times and then dried in oven at 60 °C for 6 h to obtain the final and then calcinated in a tube furnace at 700 °C for 3 h with a heating rate of 5 °C min^{-1} in air, then cooled down to room temperature naturally and the Ta_2O_5 NHs were obtained. The image of Ta_2O_5 NHs is shown in Figure S8.

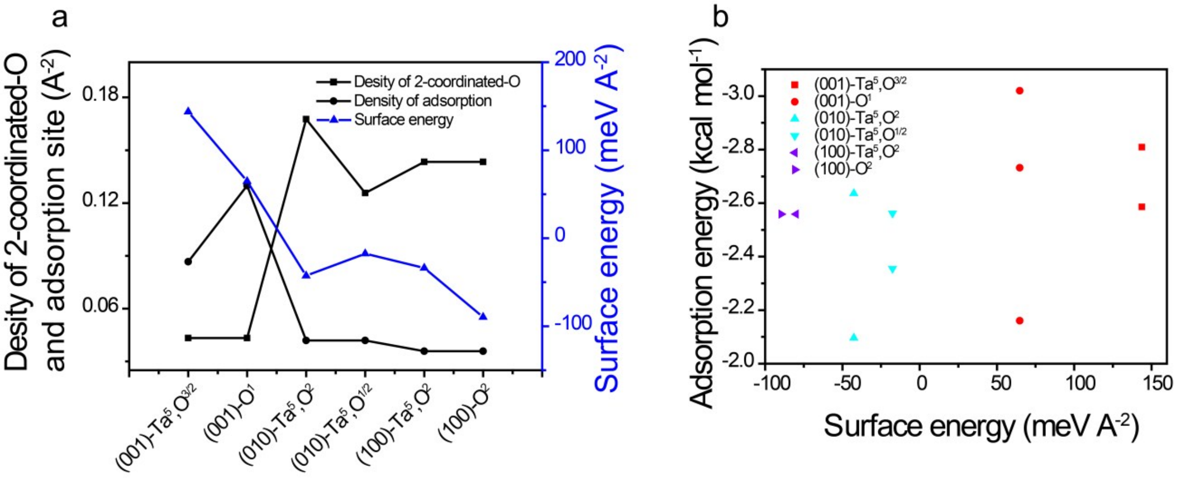

Figure S1. (a) Scatter diagram of density of 2-coordinated-O atom, adsorption site and facet energy. (b) Scatter diagram of adsorption energy and facet energy.

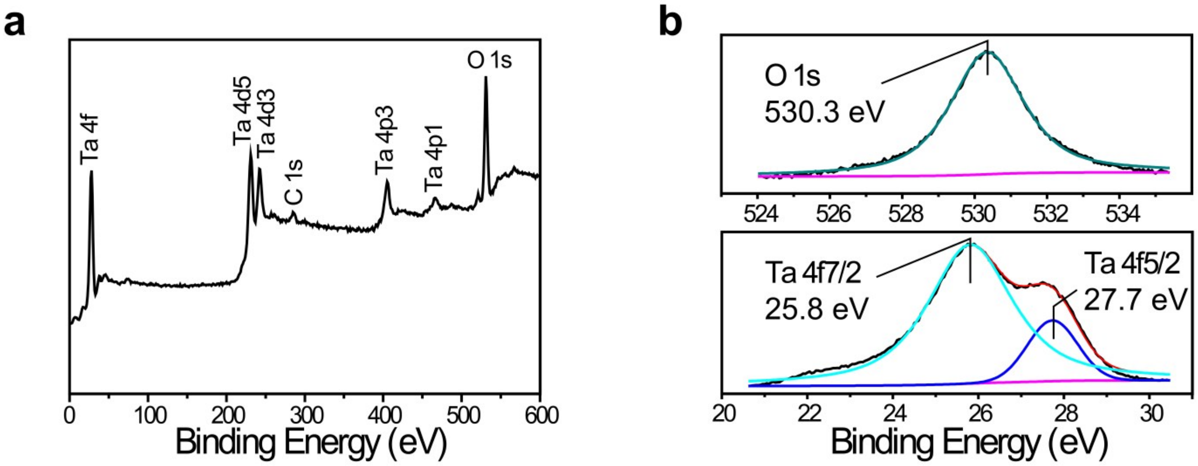

Figure S2. (a) Full and (b) O 1s and Ta 4f XPS spectra of the as-prepared Ta_2O_5 MCSCs.

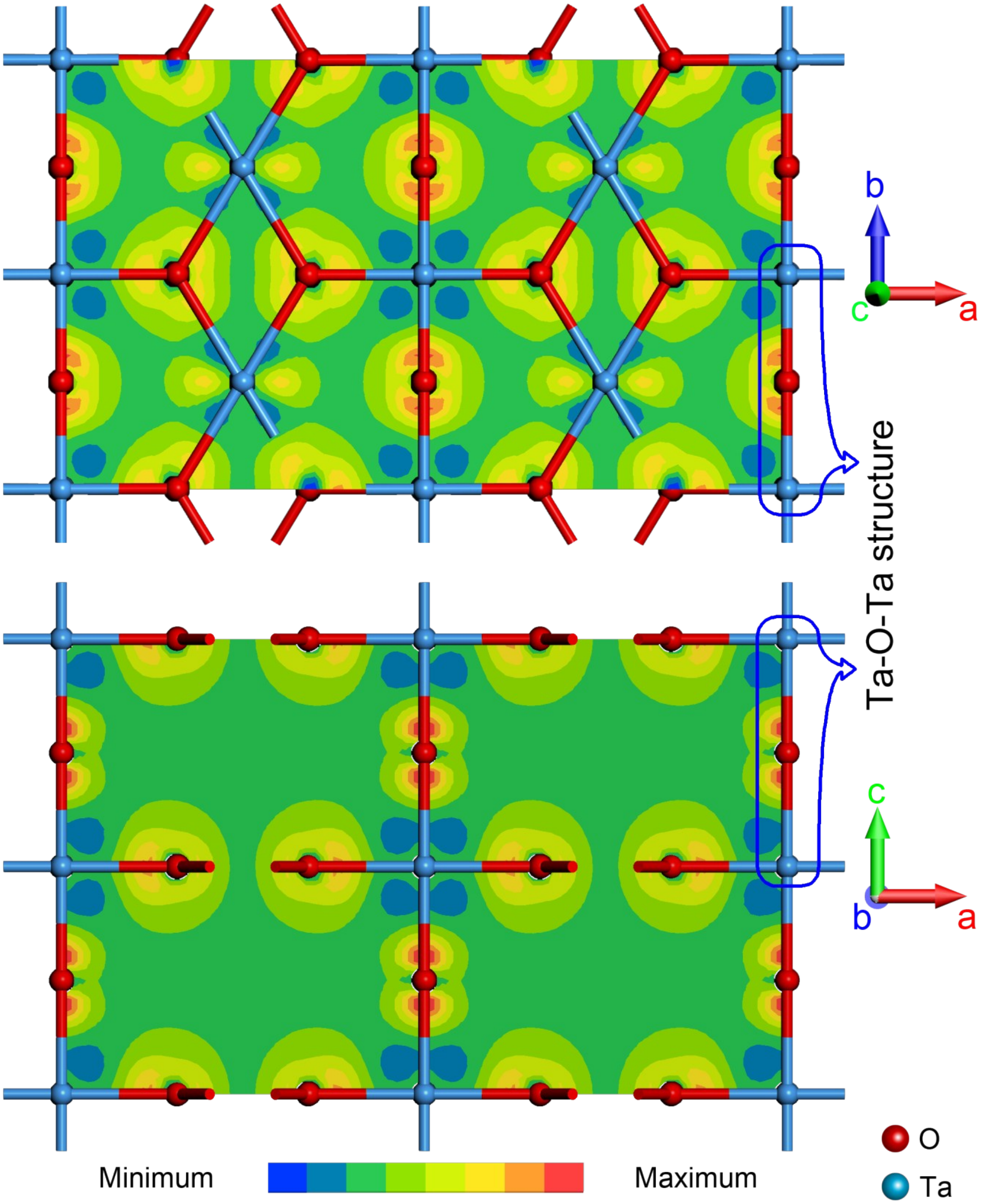

Figure S3. Electron density difference from atoms of β-Ta_2O_5.

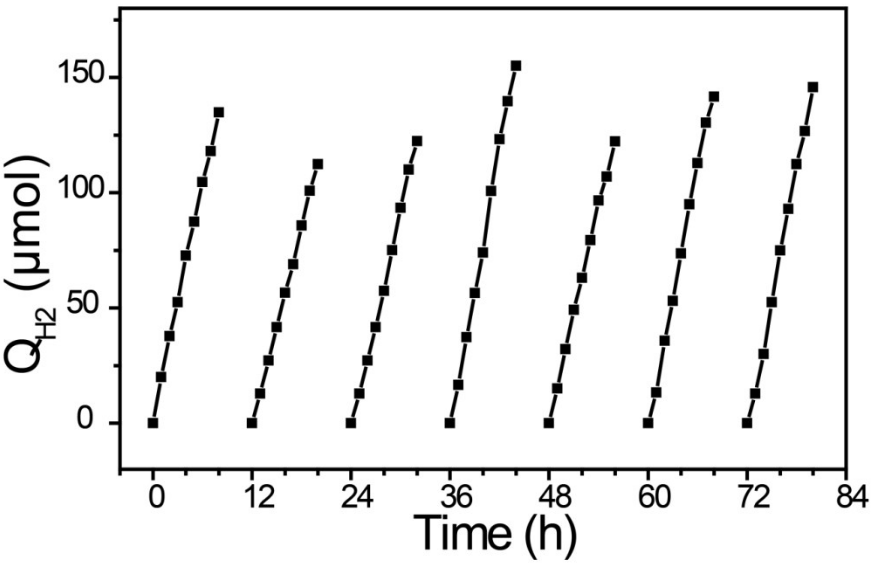

Figure S4. Cycle experiment of H_2 production.

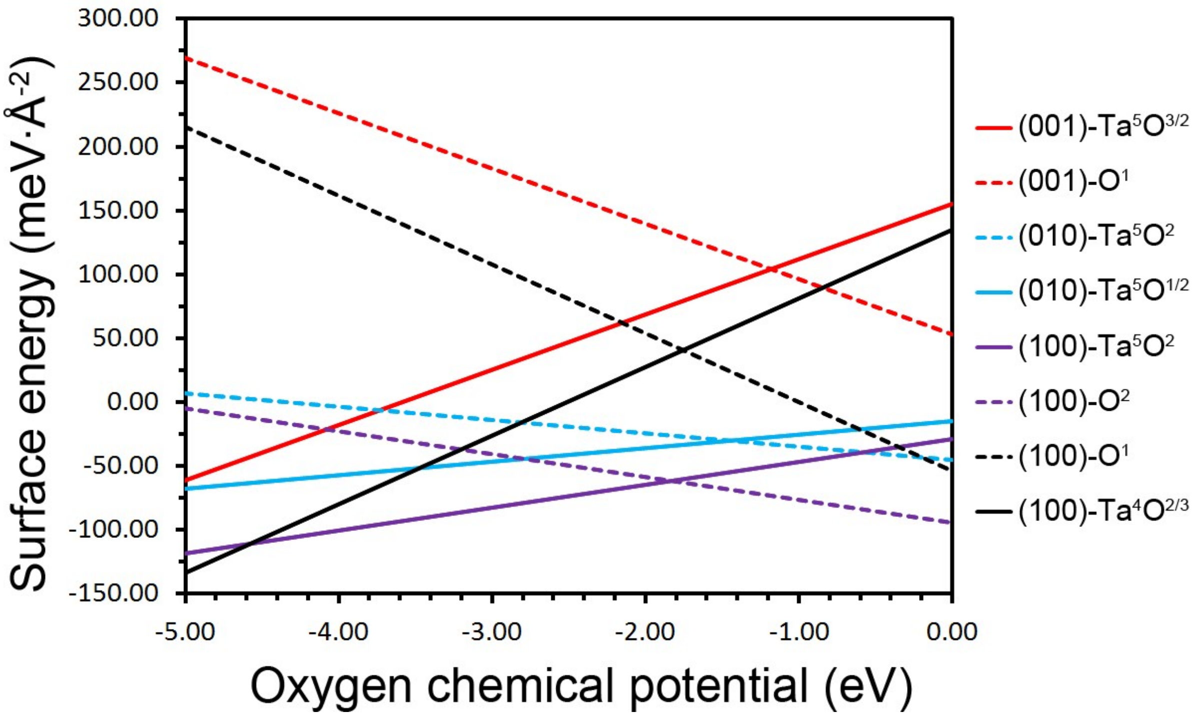

Figure S5. Facet energy range of the {001}, {010} and {100} slabs of β-Ta_2O_5.

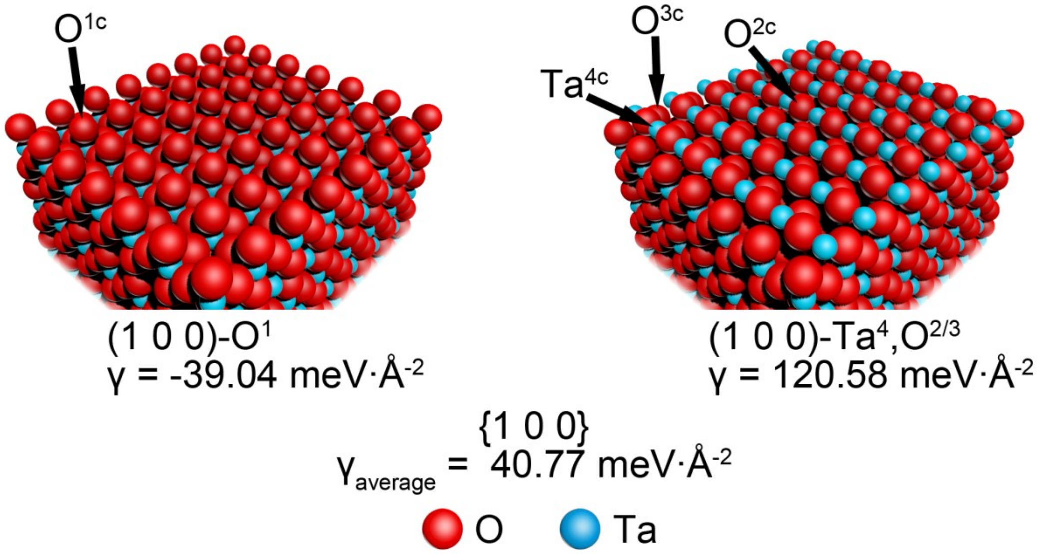

Figure S6. Illustration of the unstable terminal combination of {100} facet. The label Ta or O means the atom species. The superscripts on the right mean the coordination numbers of atoms.

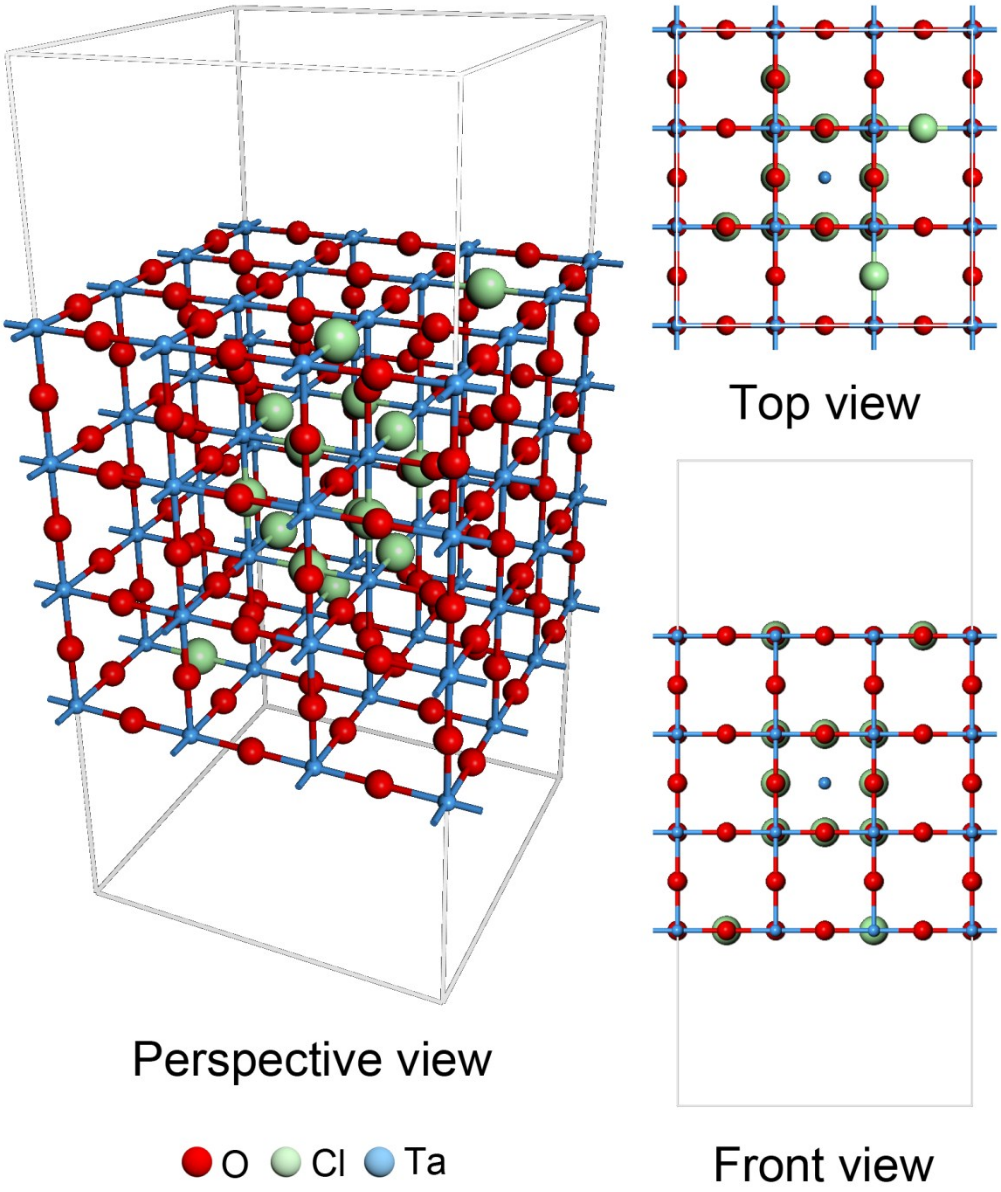

Figure S7. Illustration of slab model in dynamic simulation.

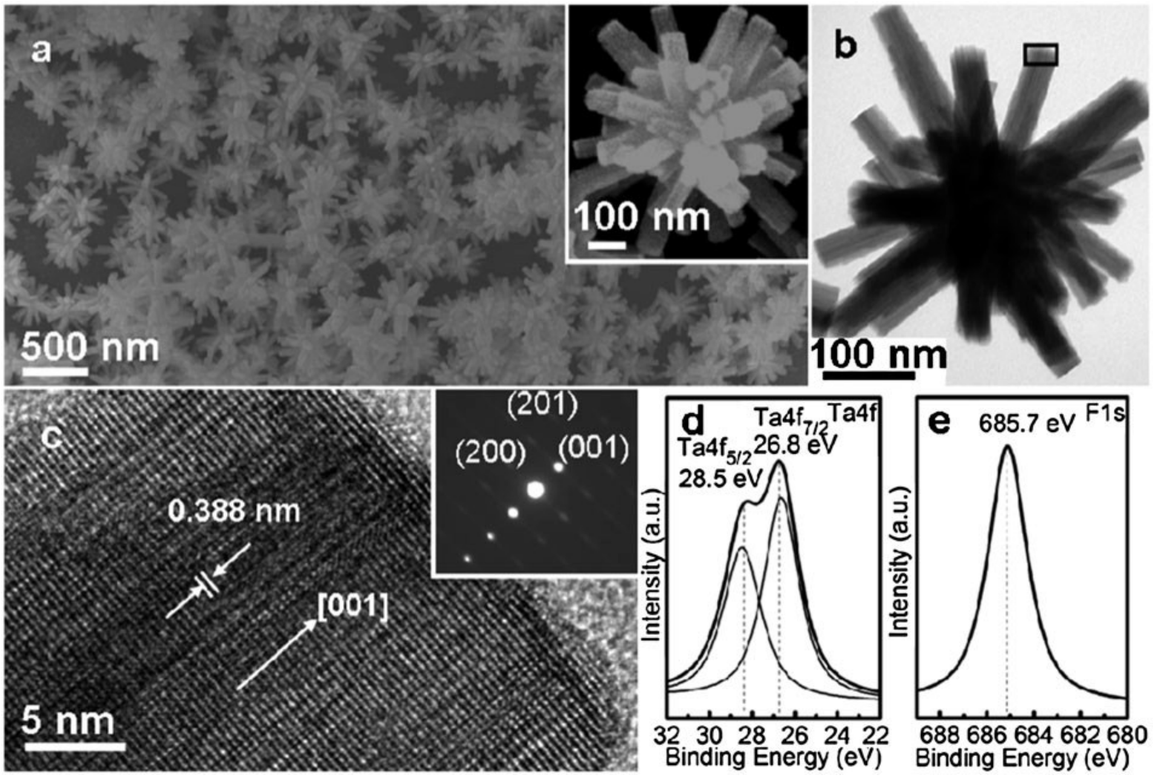

Figure S8.[13] Simple characterization of Ta_2O_5 NHs cut from reference 13.

Facet index	Facet slab	Adsorption energy (kcal·mol^{-1})	Adsorption energy Rank	Facet energy (meV·Å^{-2})	Locator illustration with in electron density difference map	Density (Å^{-2})
001	(001)-Ta^{5},O$^{3/2}$	-2.81	2	143.78	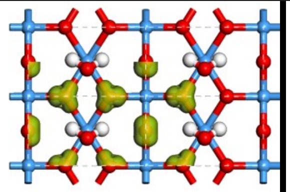	0.108
	(001)-Ta^{5},O$^{3/2}$	-2.58	5	143.78	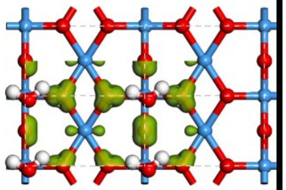	
	(001)-O^{1}	-3.02	1	64.77	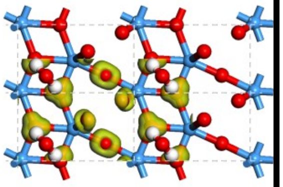	
	(001)-O^{1}	-2.73	3	64.77	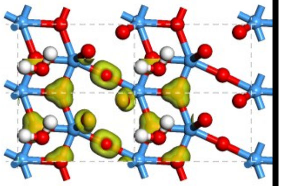	
	(001)-O^{1}	-2.16	10	64.77	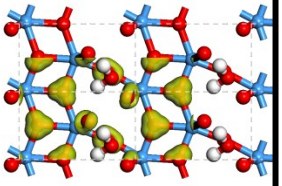	
010	(010)-Ta^{5},O^{2}	-2.64	4	-42.55	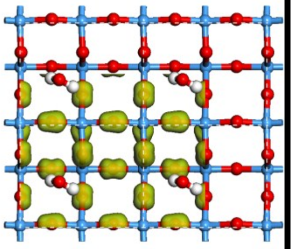	0.042

	(010)-Ta^5,O^2	-2.10	11	-42.55	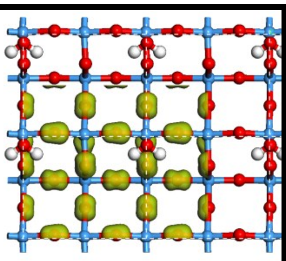	
	(010)-Ta^5,O$^{1/2}$	-2.56	7	-17.51	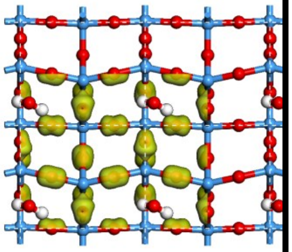	
	(010)-Ta^5,O$^{1/2}$	-2.36	9	-17.51	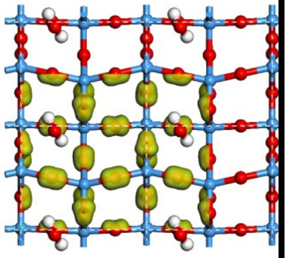	
100	(100)-Ta^5,O^2	-2.58	6	-79.99	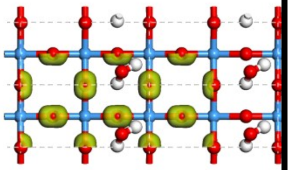	0.036
	(100)-O^2	-2.56	8	-89.64	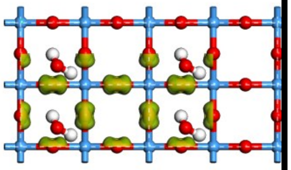	

Chart S1. Illustration of adsorption calculation details and locator of the adsorption site in the electron density difference map.

Ta ● O ●	Bulk amorphous	Intra-layer amorphous	
Molecule	Top view	Front view	Top view
Ta_4O_{10}	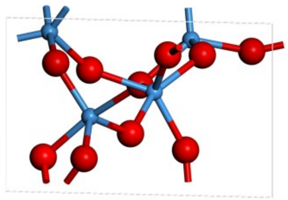	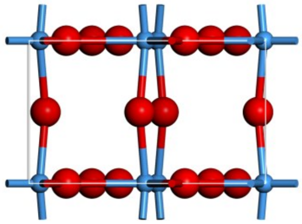	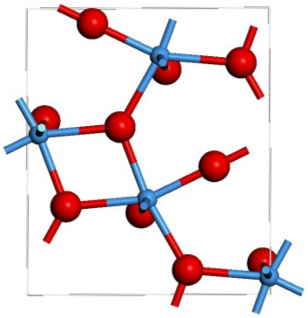
Ta_8O_{20}	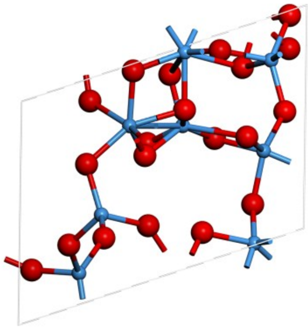	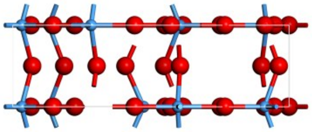	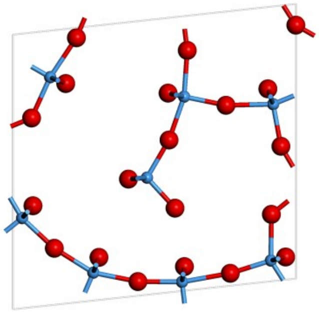
$Ta_{16}O_{40}$	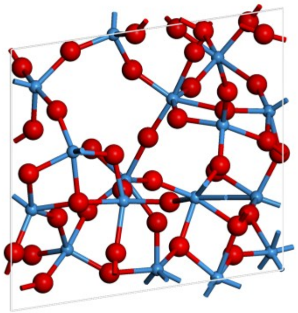	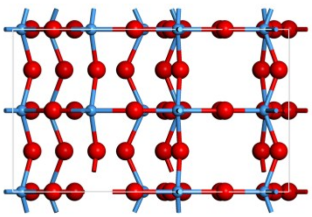	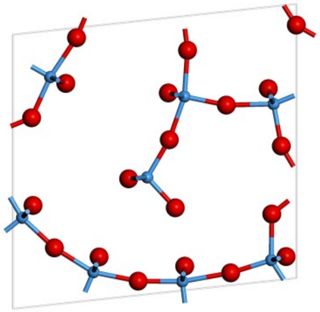

Chart S2. Illustration of bulk amorphous models and intra-layer amorphous models.

Table S1. Energies of the transition from $TaO_{2.18}Cl_{0.64}$ to Ta_2O_5 with different intermediates.

Molecule in a cell	Energy per $TaO_{2.5}$ (eV)		Molar Energy Difference $\Delta = B - I$ (kJ·mol-1)
	Bulk amorphous model (energy B)	Intra-layer amorphous model (energy I)	
Ta_4O_{10}	-1223.32	-1223.56	23.2
Ta_8O_{20}	-1223.19	-1223.46	26.1
$Ta_{16}O_{40}$	-1223.34	-1223.46	11.6
Average	-1223.28	-1223.49	20.3

Table S2. Photocatalytic H_2 production activities of the Ta_2O_5 MCSCs and NHs loaded with different amounts of Pt.

Pt loading amount (wt %)	Activity (μmol·m^{-2}·h^{-1})	
	MCSCs	NHs
0	9.06	1.94
0.5	58.86	17.86
1	86.68	36.10
3	109.31	50.47
5	115.14	56.29

Table S3. Equivalent circuits fitting of EIS Nyquist plots of the as-prepared Ta_2O_5 MCSCs and the Ta_2O_5 NHs.

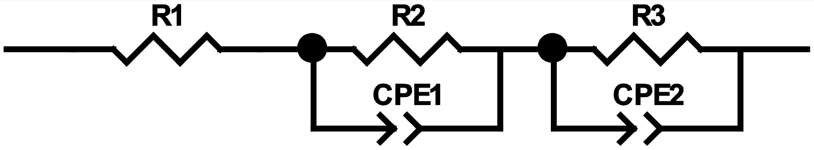

Element	MCSCs		HNs	
	Value (mho)	Error (%)	Value (mho)	Error (%)
R1	2.265	0.31467	1.812	0.40138
R2	18.27	10.195	14.35	12.764
CPE1-T	0.003503	4.3108	0.004408	4.5022
CPE1-P	0.77352	0.77371	0.77373	0.79608
R3	191.4	1.6987	153.9	1.6686
CPE2-T	0.001986	1.2558	0.002483	1.2293
CPE2-P	0.95616	1.037	0.95386	1.0738

Note: R means resistor, CPE means consistent phase element; R2 identify the interior resistance and R3 identify the boundary resistance.[14]

Table S4. Comparison of the Ta_2O_5 MCSCs and other Ta_2O_5 catalysts on photocatalytic H_2 production activity.

Catalysts	H_2 production per specific area * (μmol·m^{-2}·h^{-1})	Reference
u-Ta_2O_5	2.89	Ref. 15
Mesoporous Ta_2O_5	~3	Ref. 16
Ta_2O_5 MCSCs	8.44	This work

Note: * The photocatalytic H_2 production data listed above were obtained in a methanol aqueous solution in the absence of any cocatalysts.

Reference

1. M. C. Payne, M. P. Teter, D. C. Allan, T. Arias and J. Joannopoulos, *Rev. Mod. Phys.*, 1992, **64**, 1045.
2. W. Kohn and L. J. Sham, *Phys. Rev.*, 1965, **140**, A1133.
3. P. Hohenberg and W. Kohn, *Phys. Rev.*, 1964, **136**, B864.
4. M. D. Segall, J. D. L. Philip, M. J. Probert, C. J. Pickard, P. J. Hasnip, S. J. Clark and M. C. Payne, *J. Phys.: Condens. Matter*, 2002, **14**, 2717.
5. S. J. Clark, M. D. Segall, C. J. Pickard, P. J. Hasnip, M. J. Probert, K. Refson and M. C. Payne, *Z. Kristallogr.*, 2005, **220**, 567-570.
6. O. Dulub, U. Diebold and G. Kresse, *Phys. Rev. Lett.*, 2003, **90**.
7. K. Reuter and M. Scheffler, *Phys. Rev. B*, 2001, **65**, 035406.
8. A. Rappe, K. Colwell and C. Casewit, *Inorg. Chem.*, 1993, **32**, 3438-3450.
9. N. Metropolis, A. W. Rosenbluth, M. N. Rosenbluth, A. H. Teller and E. Teller, *Journal of Biochemical & Biophysical Methods*, 1952, **21**, 1087-1092.
10. S. Kirkpatrick, C. D. Gelatt and M. P. Vecchi, *Science*, 1983, **220**, 671-680.
11. D. Frenkel and B. Smit, 2002, **50**, 66.
12. V. Černý, *Journal of Optimization Theory & Applications*, 1985, **45**, 41-51.
13. J. Y. Duan, W. D. Shi, L. L. Xu, G. Y. Mou, Q. L. Xin and J. G. Guan, *Chem. Commun.*, 2012, **48**, 7301-7303.
14. C. Demetry and X. Shi, *Solid State Ionics*, 1999, **118**, 271-279.
15. Z. Wang, J. G. Hou, C. Yang, S. Q. Jiao, K. Huang and H. M. Zhu, *Energy Environ. Sci.*, 2013, **6**, 2134-2144.
16. L. Xu, J. Guan, W. Shi and L. Liu, *J. Colloid Interface Sci.*, 2012, **377**, 160-168.